

*Full Length Research Paper*

# Imaging flow cytometric analysis of *Schizosaccharomyces pombe* morphology

Radha Pyati<sup>1\*</sup>, Lindsay L. Elvir<sup>1</sup>, Erica C. Charles<sup>1</sup>, Umawattee Seenath<sup>1</sup> and Tom D. Wolkow<sup>2</sup>

<sup>1</sup>Department of Chemistry, University of North Florida, Jacksonville, FL 32224, USA.

<sup>2</sup>Department of Biology, University of Colorado at Colorado Springs, Colorado Springs, CO 80933, USA.

Accepted 10 March, 2011

The morphology of *Schizosaccharomyces pombe* can be rapidly monitored in asynchronous, G2-rich populations using imaging flow cytometry (IFC). Cell morphology was analyzed in terms of length and aspect ratio before and after exposure to several toxins. The toxins target the DNA (hydroxyurea and phleomycin) or cytoskeletal elements (thiabendazole, carbendazim and latrunculin A) and exert well-characterized effects on the morphology. Using IFC and yeast mutants, predictable morphological changes were detected accompanied with loss of gene products required during cellular responses to these toxins. IFC is a sensitive tool for accurate detection of subtle morphological changes in large, asynchronous *S. pombe* populations.

**Key words:** Imaging flow cytometry, fission yeast, *Schizosaccharomyces pombe*, cell cycle, morphology, genotoxin, cytoskeletal toxin.

## INTRODUCTION

Changes in cell morphology accompany the development of prokaryotic and eukaryotic cells (Singh and Montgomery, 2011; Watanabe and Takahashi 2010). Changes in cell morphology also accompany genomic instability, as morphology is linked to mechanisms that influence chromosome stability of both cell types (Gisselsson, 2002; Moseley and Nurse, 2010). Therefore, identifying the molecular processes that influence morphology is important for understanding normal and abnormal developmental processes (Lleonart et al., 2000). *Schizosaccharomyces pombe*, or fission yeast, is a very good model system for studying cell morphology (Moseley and Nurse, 2010; La Carbona et al., 2006). *S. pombe* are cylindrically shaped cells that grow from both ends as they proceed through the cell cycle (La Carbona et al., 2006). During the cell cycle, cell length increases from roughly 7  $\mu\text{m}$  to 12 -15  $\mu\text{m}$  while width remains

constant at 3.5  $\mu\text{m}$  (Nasim et al., 1989a). The cell cycle takes ~2.5 h to complete during exponential growth in liquid culture at 29.5°C. The majority of cells in an exponentially growing culture are in the G2 phase of the cell cycle, because it requires 70% of the cell cycle (1.75 h) to complete. Mitosis follows G2 and lasts about 5% of the cell cycle (7.5 min). Next, cytokinesis and septation divide the cytoplasm and result in the construction of new cell wall material called a septum. The G1 phase of both cells is completed in the next 15% of the cell cycle (22.5 min), before the septum is dissolved to produce two separate cells. The S-phase of both cells requires ~10% of the cell cycle (15 min) for completion and like G1, is initiated before septum dissolution (Nasim et al., 1989b).

Microtubules and actin are cytoskeletal components that play two critical roles during the cell cycle (La Carbona et al., 2006). First, they establish and maintain the linear growth axis of the yeast. Microtubules help localize actin to both ends of the cell, and actin incorporates new cell wall material at each end of the cell. Second, they are required to segregate DNA to daughter cells. Microtubules are major components of the mitotic spindle that pulls replicated sister chromatids to opposite ends of the cell. Actin is a major component of the contractile ring that then divides the cytoplasm at a

\*Corresponding author. E-mail: [radha.pyati@unf.edu](mailto:radha.pyati@unf.edu). Tel: 904-620-1918. Fax: 904-620-3535.

**Abbreviations:** AR, Aspect ratio; IFC, imaging flow cytometry; HU, hydroxyurea; MBC, carbendazim; Phleo, phleomycin; TBZ, thiabendazole.

location between the segregated sister chromatids. Together, these cytoskeletal proteins have great influence over the growth and division patterns of *S. pombe*. Successful completion of a typical cell cycle results in the formation of two cells that inherit healthy genomes. Toxins that challenge the structure of DNA or the cytoskeleton, threaten genomic stability. Genotoxins such as phleomycin and hydroxyurea compromise DNA structure and are highly mutagenic. Toxins that compromise the structures of microtubules and actin affect linear growth, as well as the division machinery that segregates sister chromatids. Microtubules are damaged by toxins such as methylbenzimidazol-2-ylcarbamate (MBC) and thiabendazole (TBZ), and actin is damaged by Latrunculin A (LatA).

To protect against the threats of such substances, fungi and other eukaryotic cells are equipped with cell cycle checkpoints (Hartwell and Weinert, 1989; Ciccia and Elledge, 2002; Pietenpol and Stewart, 2002; Carr, 1995). These checkpoints are signal transduction pathways that delay cell cycle progression following insult to the genome or the cytoskeleton. Cell cycle delay allows extra time to address damage, so that it is fixed before final separation of the two daughter cells. Checkpoints operate during the entire cell cycle stage and can delay cell cycle progression at many points, including G1/S, intra S, G2/M, intra M and cytokinesis. Checkpoint signaling and the resulting delay to cell cycle progression do not, however, inhibit cell growth, which continues during the cell cycle delay and results in abnormally long cells. Mutations in checkpoint *rad* genes like *rad26*<sup>+</sup> and *rad24*<sup>+</sup>, compromise these cell cycle delays and permit cell cycle progression in the presence of DNA damage or cytoskeletal damage (al-Khodairy et al., 1994; Ford et al., 1994; Carr, 1995). Toxins that target the cytoskeleton activate cell cycle checkpoints as well (Gorbsky, 1997; Lew, 2000; Gachet et al., 2006). Clearly, responses to toxins that target DNA and cytoskeletal proteins affect cell morphology. Studying cell morphology has traditionally been accomplished using optical microscopic methods. But observing the characteristics of large cell populations using optical microscopy has presented challenges in imaging thousands of particles, such as experimenter fatigue. Imaging flow cytometry (IFC) combines the high particle throughput capacity of flow cytometry with a two-dimensional imaging system to acquire images of very large cell populations in a short period of time. Both traditional and imaging flow cytometers are extremely versatile and can perform multispectral analyses (Calvert et al., 2008). However, by virtue of its ability to capture images, IFC offers a

straightforward way to conduct morphological characterization of cells, even in the absence of multispectral modes.

The aim of this work is to observe and quantify morphological changes caused by cell growth toxins of both wild-type and mutant *S. pombe*, and to do so in large, asynchronous cell populations that are difficult to

study using optical microscopy. This study reports the successful detection by IFC of predictable changes in cell length and shape that occur when asynchronous cultures of wild type and checkpoint-defective *rad26* and *rad24* strains were treated with a variety of genotoxins and cytoskeletal toxins. These results, and the promise that IFC holds for identifying compounds and defining the genes that influence cell shape in eukaryotes, are discussed. To our knowledge, this is the first report of an IFC study of fission yeast morphology.

## MATERIALS AND METHODS

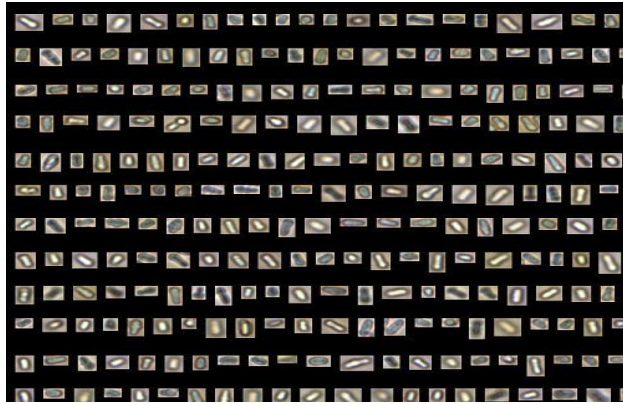
### Reagents, strains and growth conditions

YE5S media was used in this study and made from yeast extract (Becton Dickinson Bacto), dextrose (anhydrous, BDH), adenine hemisulfate dehydrate, (MP Biomedicals, Solon, Ohio), L-histidine free base (MP Biomedicals), L-leucine (MP Biomedicals), and uracil (MP Biomedicals) (Moreno et al., 1991). The toxins and stock solutions used in this study were 200 mM hydroxyurea in water (HU; MP Biomedicals), 8 mg/ml carbendazim (MBC; Aldrich, Belgium), 20 mg/ml thiabendazole (TBZ; MP Biomedicals), 5 mg/ml phleomycin (phleo, Invivogen, San Diego, CA) and 100 μM latrunculin A (LatA, Biomol International, Plymouth Meeting, PA). All stock solutions were in DMSO, unless otherwise noted. Five strains were used in this study. Two *rad26*<sup>+</sup> wild-type strains were used; these were designated 236, with genotype *leu1-32, ura4-d18, h*<sup>-</sup> and 696, with genotype *leu1-32, ura4-d18, h*<sup>+</sup>. Two *rad26Δ* strains were used, designated 257, with genotype *rad26::ura*<sup>+</sup>, *ura4-d18, h*<sup>+</sup>; and 1001, with genotype *rad26::ura*<sup>+</sup>, *ura4-D18, leu1-32, ade6-704, h*<sup>-</sup>. One *rad24Δ* strain was used, designated 466 with genotype *rad24::ura4+*, *ade*<sup>-</sup>, *leu*<sup>-</sup>, *ura*<sup>-</sup>, *h*<sup>-</sup>.

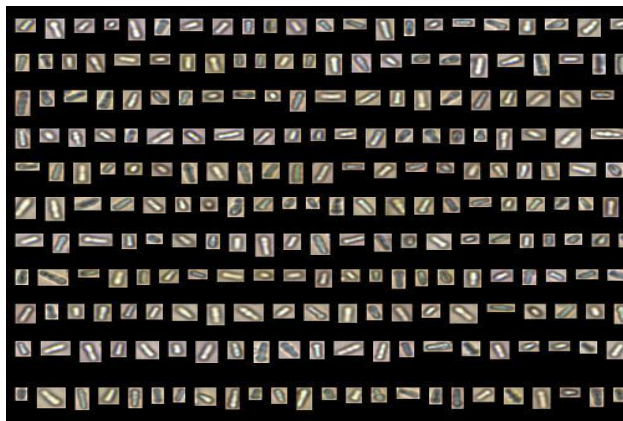
Cells stored on agar at 4°C were initially cultured overnight in liquid YE5S media at 30°C and 120 rpm for 24 h. After incubation, optical density (OD) at 595 nm was measured using liquid YE5S media as a blank. Following starter culture, transfer volumes and growth times for final samples were carefully controlled in order to obtain OD<sub>595</sub> values between 0.2 and 0.9, so that log-phase growth and sufficient cell populations could emerge, but plateau-stage growth and the accompanying senescence and exhaustion of media nutrients would not take place. Cell populations were asynchronous. The transfer volume ( $V_{transfer}$ ) was calculated using the OD<sub>595</sub> obtained from the starter culture and the formula as follows:

$$V_{TRANSFER} = \frac{0.3}{ACTUALOD2} \left( \frac{1}{OD_{IV-1}^{FINAL}} \right)^{V_{TRANSFER}} \quad \text{WHERE } N = \frac{t_{incub}}{t_{gen}}$$

The transfer volume was then halved or cut into thirds as needed. This  $V_{transfer}$  was added into 5 ml of YE5S media and incubated at 30°C and 120 rpm for a minimum of 12 h. Following this uniform growth period, OD<sub>595</sub> was measured again. If OD<sub>595</sub> exceeded 0.3, the sample was diluted with media in order to achieve an OD<sub>595</sub> of 0.3, to ensure that plateau growth and senescence did not occur during the 3-h period of toxin exposure. After any necessary dilution, samples were left untreated or treated with 10 mM HU, 8 μg/ml MBC, 20 μg/ml TBZ, 0.2 μM LatA, or 7.5 μg/ml phleo for 3 h. The untreated samples served as control samples that did not have any toxin added but underwent the same OD measurement, dilution, and 3-h growth period. OD<sub>595</sub> was measured once more to ensure that all final OD<sub>595</sub> values lay between 0.2 and 0.9. The samples were centrifuged at 5000 rpm for 2 min, washed in



466 Control



236 Control

**Figure 1.** Representative cell image data for a minimum of 10,000 cell images per run captured by FlowCAM imaging flow cytometer (IFC). The IFC directs the cell suspension through a 50- $\mu\text{m}$  flow cell positioned in front of a 20X objective and a camera that captures real-time images of the particles in the fluid as they pass through the flow cell. Each image is stored separately along with up to 26 individual particle measurements, including length and aspect ratio, for each image. Each run was set to stop upon reaching 40,000 particle images. These were then filtered to remove undesirable images like partial cells, blurry images, and multiple cells to leave a minimum of 10,000 images for each experiment. A table containing 26 parameters for each cell was exported to Microsoft Excel, within which median values of length and aspect ratio were calculated.

phosphate buffered saline (0.2 M Phosphate, 1.5 M NaCl), aspirated, centrifuged again, and resuspended in 70% cold ethanol to preserve samples. The samples were stored at 4°C until ready for flow cytometric analysis.

### Imaging flow cytometry

Samples in ethanol were resuspended in PBS for analysis using the image flow cytometer. Samples underwent two cycles of the following: centrifugation at 5,000 rpm for 2 min, removal of supernatant, dilution in PBS, aspiration, and vortexing to break-up cell clumps. Final samples in PBS were incubated for 30 min prior to flow cytometric analysis. Five to seven drops of the sample

solution was placed into the opening of the FlowCAM imaging flow cytometer (Fluid Imaging Technologies, Yarmouth, ME). Figure 2 depicts the FlowCAM imaging flow cytometer (IFC). The fluidics system uses a peristaltic pump to pull the fluid sample through a flow cell perpendicular to the optical path. In this study, the pump was set to a value of 8. Each run was set to stop upon reaching 40,000 particle images. Fluorescence detection was not used in this study.

### Data analysis

In each experiment, 40,000 images were rapidly collected and then filtered to remove undesirable images like partial cells, blurry images, and multiple cells to leave a minimum of 10,000 images for each experiment. One more filtering step was done by creating a library of cell images that possessed the general shape of fission yeast cells but included a wide range of lengths and aspect ratios. A table containing 26 parameters for each cell was exported to Microsoft Excel. The two parameters of interest in this work were length and aspect ratio; median values of these were calculated in Excel. Triplicate trials of each experiment yielded average values of these, along with standard deviations for each.

## RESULTS AND DISCUSSION

### Cell length and aspect ratio

Figure 1 shows two representative examples of image data collected in this study. The two collages of cell images show a random sample of cell images for strains 236 (wild-type) and 466 (*rad24*). Table 1 shows results for cell length and aspect ratio for all strains, including untreated-control and toxin-exposed. Comparison between control and toxin-exposed was done by calculating percent change in a given parameter relative to control. For example, percent change in median cell length ( $PC_L$ ) relative to the control was calculated by the formula:

$$PercentChange = \left( \frac{L_{toxin} - L_{control}}{L_{control}} \right) * 100$$

Standard deviations for  $PC_L$  were obtained using the standard deviations for both  $L_{toxin}$  and  $L_{control}$  and a partial derivative method that incorporates both errors (Mortimer, 1981). Aspect ratio was handled in the same manner. Percent change values are also displayed in Table 1. Figures depicting these results are shown with error bars consisting of that calculated standard deviation above and below the median; these appear large because the plot shows percent change, not percent of  $L_{control}$ .

### Cell length

IFC was used to measure the cell length of five different strains: two *rad*<sup>+</sup> strains, two *rad26* strains and one

**Table 1.** Cell lengths and aspect ratios, and percent change in median cell length and median aspect ratio of toxin study.

Sample	Median cell length (um)	Percent change in median cell length relative to control (%)	Median aspect ratio	Percent change in median aspect ratio relative to control (%)
<b>Rad<sup>+</sup> (wild-type)</b>				
236Control	7.20 ± 0.37	--	0.47 ± 0.03	--
236Phleo	11.23 ± 1.26	56.0 ± 19.2	0.29 ± 0.07	-38.7 ± 15.3
236HU	7.87 ± 0.20	9.3 ± 6.3	0.45 ± 0.01	-5.6 ± 5.6
236TBZ	7.59 ± 0.05	5.4 ± 5.5	0.45 ± 0.02	-4.2 ± 6.7
236MBC	7.20 ± 0.16	0.0 ± 5.6	0.48 ± 0.03	0.7 ± 7.5
236LatA	8.31 ± 1.20	15.4 ± 17.7	0.45 ± 0.06	-5.6 ± 13.0
696Control	8.01 ± 0.06	--	0.43 ± 0.01	--
696Phleo	11.84 ± 0.43	47.8 ± 5.5	0.22 ± 0.02	-48.5 ± 3.6
696HU	8.95 ± 0.23	11.7 ± 3.0	0.39 ± 0.02	-10.0 ± 4.8
696TBZ	8.29 ± 0.09	3.5 ± 1.4	0.38 ± 0.00	-12.3 ± 1.2
696MBC	8.15 ± 0.08	1.7 ± 1.3	0.40 ± 0.01	-6.9 ± 1.8
696LatA	10.44 ± 0.07	30.3 ± 1.3	0.38 ± 0.01	-12.3 ± 2.6
<b>Rad26</b>				
257Control	7.47 ± 0.08	--	0.46 ± 0.00	--
257Phleo	7.12 ± 0.03	-4.7 ± 1.1	0.47 ± 0.00	2.2 ± 0.0
257HU	7.04 ± 0.07	-5.8 ± 1.4	0.49 ± 0.01	6.5 ± 2.2
257TBZ	7.57 ± 0.10	1.3 ± 1.7	0.46 ± 0.01	-0.7 ± 1.3
257MBC	7.32 ± 0.09	-2.0 ± 1.6	0.46 ± 0.01	0.0 ± 2.2
257LatA	9.06 ± 0.12	21.3 ± 2.1	0.43 ± 0.01	-7.2 ± 1.3
1001Control	7.03 ± 0.59	--	0.51 ± 0.05	--
1001Phleo	6.94 ± 0.16	-1.3 ± 8.6	0.53 ± 0.02	4.6 ± 11.1
1001HU	7.12 ± 0.10	1.3 ± 8.6	0.58 ± 0.01	13.1 ± 11.7
1001TBZ	7.19 ± 0.21	2.3 ± 9.1	0.52 ± 0.02	2.0 ± 10.9
1001MBC	7.09 ± 0.45	0.9 ± 10.6	0.55 ± 0.03	8.5 ± 12.7
1001LatA	9.72 ± 0.32	38.3 ± 12.5	0.46 ± 0.01	-9.2 ± 9.3
<b>Rad24</b>				
466Control	6.68 ± 0.09	--	0.58 ± 0.01	--
466Phleo	6.64 ± 0.07	-0.6 ± 1.7	0.60 ± 0.01	2.9 ± 2.7
466HU	6.03 ± 0.13	-9.7 ± 2.3	0.63 ± 0.01	8.6 ± 2.5
466TBZ	6.37 ± 0.04	-4.6 ± 1.4	0.66 ± 0.02	13.2 ± 4.1
466MBC	6.24 ± 0.55	-6.6 ± 8.3	0.61 ± 0.00	5.2 ± 1.8
466LatA	8.86 ± 0.03	32.6 ± 1.8	0.50 ± 0.01	-14.4 ± 1.8

Values given are means of three replicates ± S.D. (each trial contains 10,000 cells minimum).

*rad24* strain. Asynchronous cultures of these strains were grown in complete liquid medium to an OD between 0.2 and 0.9 before processing them for IFC. Overall, median cell length fell between 6.85 and 8.23 μm, although slight differences between strains were observed. For example, the *rad<sup>+</sup>* strains differ by 0.81 μm and the two *rad26* strains differ by 0.44 μm. Strain backgrounds therefore affect cell length. Next, asynchronous cultures of each strain were treated for 3 h with five different toxins, each of which activates a cell cycle checkpoint mechanism that delays cell cycle progression

but not cell growth. These toxins may be categorized by similar mechanisms of action, but within each category, differences exist between toxins. Their effects are shown in Figure 2A. Phleo and HU are both genotoxins that delay progression from G<sub>2</sub> into mitosis by *rad<sup>+</sup>*-dependent mechanisms (Enoch and Nurse, 1990; Baschal et al., 2006) however, they operate in different ways. Phleo causes DNA breaks (Sleigh and Grigg, 1977) and damages DNA throughout the 2.5 h cell cycle, including G<sub>2</sub>, where ~70% of cells in an asynchronous culture reside. Following treatment with phleo, those cells closest

to the G<sub>2</sub>/M boundary will delay entry into mitosis sooner than those cells that are positioned earlier in the cell cycle. After 3 h of treatment, the cells closest to the G<sub>2</sub>/M boundary when the drug was added should therefore be longer than those that were in early G<sub>2</sub> or S-phase when the drug was added. The ~5% of cells in mitosis, when phleo was added, will display very little elongation, since these require another ~2 h 22 min (95% of 2.5 h) of growth before they reach the G<sub>2</sub>/M boundary. HU, on the other hand, alters deoxyribonucleoside triphosphate pools and blocks DNA synthesis (Bianchi et al., 1986). In an asynchronous culture, HU only affects ~10% of cells that are in S-phase and causes them to delay at the G<sub>2</sub>/M boundary. Those cells in G<sub>2</sub> at the time of HU addition will divide and enter S-phase of the next cell cycle, at which point HU will affect their DNA synthesis. Therefore, HU should have a less pronounced effect on cell length when compared to phleo.

As anticipated, phleo caused wild type cells to elongate 45 to 55% of control length while HU caused them to elongate ~10% of control length. Also as anticipated, the three *rad* strains lacking a functional G<sub>2</sub>/M checkpoint failed to display significant elongation. LatA is a toxin that inhibits polymerization of actin microfilaments (Coue et al., 1987) and at low concentration, blocks actomyosin-based contractile ring function in *S. pombe* without significantly affecting elongation (Liu et al., 2000). Cells treated with LatA complete mitosis, but due to an inability to complete cytokinesis, are delayed for entry into mitosis of the following cell cycle. In liquid culture, this delay eventually results in a large population of elongated cells with two G<sub>2</sub> nuclei. Since this delay is dependent upon Rad24, *rad24* cells undergo multiple nuclear divisions during LatA treatment but continue to elongate due to an inability to perform cytokinesis. Therefore, elongated and multinucleated cells are produced when a culture of *rad24* cells is treated with LatA. As expected, in this study, LatA treatment caused elongation of all strains to, 15 to 38% of the control. The fact that LatA's effect on length was less than phleomycin and greater than hydroxyurea is consistent with expectation, because LatA blocks cytokinesis, a cell cycle event that occurs between G<sub>2</sub> and S-phase.

TBZ and MBC are both microtubule drugs that disrupt microtubule polymerization in dose-dependent manners. Snaith and Sawin (2003) observed that MBC is a more potent inhibitor that almost completely disrupts microtubule architecture at doses above 15 to 20 µg/ml, while TBZ fails to completely disrupt this architecture at the extremely high doses of 100 µg/ml. MBC is also more specific than TBZ, which disrupts actin polarity determinants that remain unperturbed during MBC treatment (Snaith and Sawin, 2003). Using elutriation to produce a synchronous population of wild-type cells, Snaith and Sawin observed that TBZ inhibited cell elongation and MBC did not. In the present study, little change in the length of wild-type or *rad* strains was

observed after both 3 h treatments. These inconsistencies most likely reflect experimental procedures; much lower concentrations of MBC (8 µg/ml) and TBZ (20 µg/ml) were used in this work. Overall, phleo produced the greatest effect on wild-type cell length because it can affect cells in G<sub>2</sub>. LatA produced the next greatest effect on cell length, because it targets the actin machinery required for cytokinesis, followed by HU that targets S-phase cells. TBZ and MBC produced little change in cell length.

### Cell aspect ratio

Cell aspect ratio (AR) is also a useful measure of cellular morphology. AR is defined in this work as a unitless quantity equal to the width of the cell divided by its length. The pattern recognition software in the FlowCAM instrument identifies length as the longest dimension of a cell, and width as the shortest dimension. Generally cells like *S. pombe* that are shaped like a cylinder have an aspect ratio of less than one. An AR of one represents a circular or square object. The higher the AR, or the closer it approaches one, the more rounded the cell morphology. The lower the AR, or the further from one, the more elongated the morphology. Rad24 is a 14-3-3 protein required during responses to DNA damage and both microtubule and actin cytoskeleton damage (Ford et al., 1994; Mishra et al., 2005; Baschal et al., 2006; van Heusden and Steensma, 2006). It also functions to help regulate a pheromone signaling pathway that regulates a switch from mitotic to meiotic division (Ozoe et al., 2002). Due to one or a combination of these roles, loss of *rad24* results in a striking cone-shaped spherical morphology (Ford et al., 1994). Rad26 is a coiled-coil protein that responds to structural abnormalities of DNA and the microtubule cytoskeleton (al-Khodairy et al., 1994; De Souza et al., 1999; Herring et al., 2010). Loss of its microtubule-related role by the *rad26.4a* allele results in the production of shorter cells that retain their cylindrical shape but have slightly altered length/width ratios (L/W = 2.06, AR = W/L = 0.485) when compared to wild-type cells (L/W = 2.53, AR = W/L = 0.395) (Herring et al., 2010).

Therefore, both *rad24* and *rad26* cells have altered morphologies although *rad24* cells have a more rounded appearance. AR measurements confirmed that *rad24* cells were the most spherical (AR = 0.58), while strain differences prevent a comparison of the ARs of the two wild-type and *rad26* strains. As expected, both wild-type strains retain their cylindrical appearances following all five toxin treatments, although strain differences were apparent (Figure 2B). The *rad26* and *rad24* strains become more spherical following phleo and HU, likely because a population of the asynchronous cells fail to arrest division and instead divides to produce short, dead cells in the presence of these drugs. It is not clear why

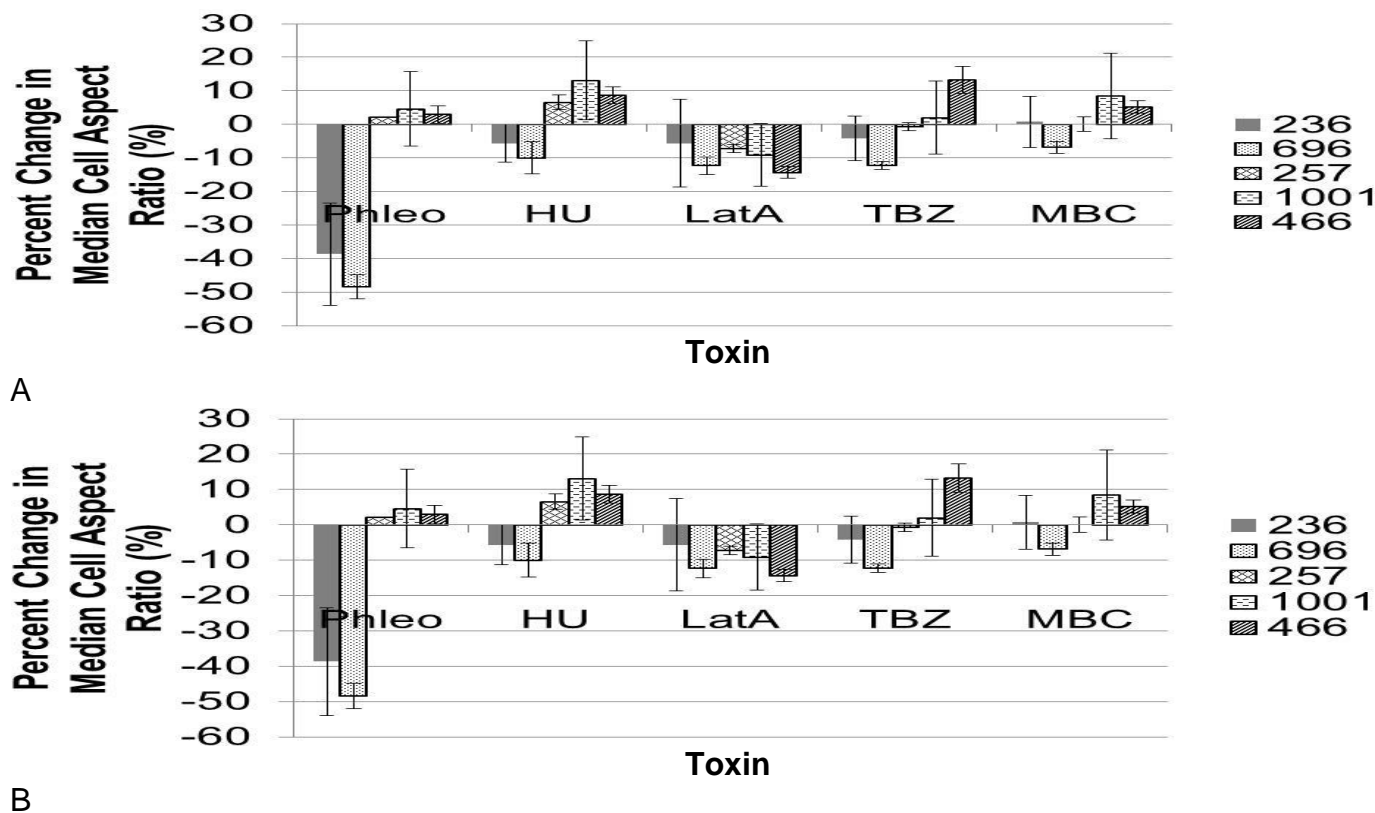


**Figure 2.** A) Percent change in median cell length versus toxin. Error bars represent one calculated standard deviation above and below the median. B) Percent change in median aspect ratio versus toxin. Error bars represent one calculated standard deviation above and below the median.

they become more spherical following HU treatment compared to phleo treatment. These genes may be required to preserve cylindrical morphology after replication forks are stalled, considering that budding yeast checkpoint proteins have been shown to control cell morphology during HU treatment (Enserink et al., 2006). Changes in the ARs of the *rad* strains differed following MBC and TBZ treatments, consistent with the observation that TBZ targets processes in addition to those targeted by MBC. For example, TBZ increases the AR of the *rad24* by 13%, while MBC increases it by 6%. On the other hand, TBZ only increases the AR of the 1001 *rad26* by 2%, while MBC increases the AR of this strain by almost 9%. The AR of the 257 *rad26* strain does not change following either TBZ or MBC treatment. Not surprisingly, none of the strains becomes more spherical during LatA treatment, which at this low dose targets the cytotkinetic machinery only.

In summary, the purpose of this study was to determine if IFC can be used to monitor two morphological characteristics, length and AR, of *S. pombe* cells grown in asynchronous cultures. To address both characteristics, a variety of different strains were treated with a variety of different toxins in an effort to produce a range of predictable cell lengths and ARs. With respect to

monitoring length, IFC was able to capture differential increases in cell length that occur when wild-type and *rad* cells are treated with drugs that target different cell structures at different cell cycle positions (Figure 2A). Likewise, IFC also captured the spherical appearances of untreated *rad24* cells and toxin-treated *rad* cells (Figure 2B). We conclude that IFC is a reliable technique that can monitor these two morphological characteristics of *S. pombe*.

### Applications of IFC using *S. pombe*

IFC may prove useful for linking molecular characteristics of cells to their morphology in two different ways. First, it may be used to rapidly screen synthetic or natural product chemical libraries for small molecules that affect cell length or AR. Those that affect length will likely target essential cellular structures, like DNA or the contractile ring, and result in cell cycle delays and concomitant increases in cell length. The extent of length increase should also help define the point in the cell cycle where drugs act. Routine genetic screens can then be performed to identify the target of this small molecule. Such small molecules may have use in basic and

translational biomedical research. IFC may also be used to rapidly screen *S. pombe* mutant collections in search of those with elevated ARs.

This would lead to the identification of non-essential genes, like *rad24*<sup>+</sup>, that influence cell shape and would otherwise be very difficult to identify using laborious genetic methods (Verde et al., 1995). While IFC cannot replace sophisticated high-throughput image capture platforms used to study more complex organisms (Shamir et al., 2010). It can be used to study the relatively simple morphology of single celled model organisms like yeast in search of evolutionarily conserved mechanisms that regulate eukaryotic morphology.

## ACKNOWLEDGEMENT

The authors thank the University of North Florida for supporting this work.

## REFERENCES

- al-Khodairy F, Fotou E, Sheldrick KS, Griffiths DJ, Lehmann AR, Carr AM (1994). Identification and characterization of new elements involved in checkpoint and feedback controls in fission yeast. *Mol. Biol. Cell.*, 5(2): 147-60.
- Baschal EE, Chen KJ, Elliott LG, Herring MJ, Verde SC, Wolkow TD (2006). The fission yeast DNA structure checkpoint protein RAD26<sup>ATRIP/LCBI/UVSD</sup> accumulates in the cytoplasm following microtubule destabilization, *BMC Cell Biol.*, 7:32.
- Bianchi V, Pontis E, Reichard P (1986). Changes of deoxyribonucleoside triphosphate pools induced by hydroxyurea and their relation to DNA synthesis. *J. Biol. Chem.*, 261: 16037-16042.
- Calvert MEK, Lannigan JA, Pemberton LF (2008). Optimization of yeast cell cycle analysis and morphological characterization by multispectral imaging flow cytometry. *Cytometry Part A*, 73A: 825-833.
- Carr AM (1995). DNA structure checkpoints in fission yeast. *Semin. Cell Biol.*, 6: 65-72.
- Ciccio A, Elledge SJ (2002). The DNA Damage Response: Making It Safe to Play with Knives. *Mol. Cell.*, 40: 179-204.
- Coue M, Brenner SL, Spector I, Korn ED (1987). Inhibition of actin polymerization by latrunculin A. *FEBS Lett.*, 213: 316-318.
- De Souza CP, Ye XS, Osmani SA (1999). Checkpoint defects leading to premature mitosis also cause endoreplication of DNA in *Aspergillus nidulans*. *Mol. Biol. Cell.*, 10: 3661-3674.
- Enoch T, Nurse P (1990). Mutation of fission yeast cell cycle control genes abolishes dependence of mitosis on DNA replication. *Cell*, 60: 665-73.
- Enserink JM, Smolka MF, Zhou H, Kolodner RD (2006). Checkpoint proteins control morphogenetic events during DNA replication stress in *Saccharomyces cerevisiae*. *J. Cell Biol.*, 175: 729-741.
- Ford JC, al-Khodairy F, Fotou E, Sheldrick KS, Griffiths DJ, Carr AM (1994). 14-3-3 protein homologs required for the DNA damage checkpoint in fission yeast. *Science*, 265: 533-535.
- Gachet Y, Reyes C, Goldstone S, Tournier S (2006). The fission yeast spindle orientation checkpoint: A model that generates tension? *Yeast*, 23(13): 1015-1029.
- Gisselsson D (2002). Tumour morphology – interplay between chromosome aberrations and founder cell differentiation. *Histol. Histopathol.*, 17: 1207-1212.
- Gorsky GJ (1997). Cell cycle checkpoints: arresting progress in mitosis. *Bioessays*, 19(3): 193-197.
- Hartwell LH, Weinert TA (1989). Checkpoints: controls that ensure the order of cell cycle events. *Science*, 246: 629-634.
- Herring M, Davenport N, Stephan K, Campbell S, White R, Kark J, Wolkow TD (2010). Fission yeast RAD26/ATRIP delays spindle-pole-body separation following interphase microtubule damage. *J. Cell Sci.*, 123(Pt 9): 1537-1545.
- La Carbona S, Le Goff C, LeGoff X (2006). Fission yeast cytoskeletons and cell polarity factors: connecting at the cortex. *Biol. Cell*, 98: 619-631.
- Lew DJ (2000). Cell-cycle checkpoints that ensure coordination between nuclear and cytoplasmic events in *Saccharomyces cerevisiae*. *Curr. Opin. Genet. Dev.*, 10(1): 47-53.
- Liu J, Wang H, Balasubramanian, MK (2000). A checkpoint that monitors cytokinesis in *Schizosaccharomyces pombe*. *J. Cell Sci.*, 113: 1223-1230.
- Lleonart ME, Martin-Duque P, Sanchez-Prieto R, Moreno A, Ramon y, Cajal S (2000). Tumor heterogeneity: morphological, molecular and clinical implications. *Histol. Histopathol.*, 15: 881-898.
- Mishra M, Karagiannis J, Sevugan M, Singh P, Balasubramanian MK (2005). The 14-3-3 protein rad24p modulates function of the cdc14p family phosphatase clpp/flpp in fission yeast. *Curr. Biol.*, 15: 1376-1383.
- Moreno S, Klar A, Nurse P (1991). Molecular genetic analysis of fission yeast *Schizosaccharomyces pombe*. *Methods Enzymol.*, 194: 795-823.
- Mortimer RG (1981). *Mathematics for physical chemistry*. Macmillan Publishing Co., Inc., New York, p. 280.
- Moseley JB, Nurse, P (2010). Cell division intersects with cell geometry. *Cell*, 142: 184-188.
- Nasim A, Young PG, Johnson BF (1989a). Editors, *Molecular Biology of the Fission Yeast (Cell Biology Series)*. New York: Academic Press, New York, p. 332.
- Nasim A, Young PG, Johnson BF (1989b). Editors, *Molecular Biology of the Fission Yeast (Cell Biology Series)*. New York: Academic Press; New York, 1989, p 217.8a.
- Ozoe F, Kurokawa R, Kobayashi Y, Jeong HT, Tanaka K, Sen K, Nakagawa T, Matsuda H, Kawamukai M (2002). The 14-3-3 proteins Rad24 and Rad25 negatively regulate Byr2 by affecting its localization in *Schizosaccharomyces pombe*. *Mol. Cell. Biol.*, 22: 7105-7119.
- Pietenpol JA, Stewart ZA (2002). Cell cycle checkpoint signaling: cell cycle arrest versus apoptosis. *Toxicology*, 181-182: 475-481.
- Shamir L, Delaney JD, Orlov N, Eckley DM, Goldberg IG (2010). Pattern recognition software and techniques for biological image analysis. *PLoS Comput. Biol.*, 6(11): e1000974.
- Singh SP, Montgomery BL (2011). Determining cell shape: regulation of cyanobacterial cellular differentiation and morphology. *Trends Microbiol.*, 19: 278-285. DOI: 10.1016/j.tim.2011.03.001.
- Sleigh MJ, Grigg GW (1977). Sulphydryl-mediated DNA breakage by pleomycin in *Escherichia coli*. *Mutat. Res.*, 42: 181-190.
- Snaith HA, Sawin KE (2003). Role of microtubules and tea1p in establishment and maintenance of fission yeast cell polarity. *J. Cell Sci.*, 117(5): 689-700.
- van Heusden GP, Steensma HY (2006). Yeast 14-3-3 proteins. *Yeast*, 23: 159-171.
- Verde F, Mata J, Nurse P (1995). Fission yeast cell morphogenesis: Identification of new genes and analysis of their role during the cell cycle. *J. Cell Biol.*, 131(6 Pt 1): 1529-1538.
- Watanabe T, Takahashi Y (2010). Tissue morphogenesis coupled with cell shape changes. *Curr. Opin. Genet. Dev.*, 20: 443-447. DOI: 10.1016/j.gde.2010.05.004.